

Article

Airborne Remote Sensing of a Biological Hot Spot in the Southeastern Bering Sea

James H. Churnside ^{1,*}, Evelyn D. Brown ², Sandra Parker-Stetter ³, John K. Horne ³, George L. Hunt, Jr. ³, Nicola Hillgruber ⁴, Michael F. Sigler ⁵ and Johanna J. Vollenweider ⁵

¹ NOAA Earth System Research Laboratory, 325 Broadway, Boulder, CO 80305, USA

² Flying Fish Ltd., P.O. Box 169, Husum, WA 98623, USA; E-Mail: flyingfishltd@embarqmail.com

³ School of Aquatic and Fishery Sciences, University of Washington, P.O. Box 355020, Seattle, WA 98195, USA; E-Mails: slps@u.washington.edu (S.P.-S.); jhorne@u.washington.edu (J.K.H.); geohunt2@uw.edu (G.L.H.)

⁴ School of Fisheries and Ocean Science, University of Alaska Fairbanks, Juneau, AK 99801, USA; E-Mail: nhillgruber@alaska.edu

⁵ NOAA Alaska Fisheries Science Center, 17109 Point Lena Loop Road, Juneau, AK 99801, USA; E-Mails: mike.sigler@noaa.gov (M.F.S.); johanna.vollenweider@noaa.gov (J.J.V.)

* Author to whom correspondence should be addressed; E-Mail: james.h.churnside@noaa.gov; Tel.: +1-303-497-6744; Fax: +1-303-497-5318.

Received: 27 January 2011; in revised form: 7 March 2011 / Accepted: 14 March 2011 /

Published: 21 March 2011

Abstract: Intense, ephemeral foraging events within localized hot spots represent important trophic transfers to top predators in marine ecosystems, though the spatial extent and temporal overlap of predators and prey are difficult to observe using traditional methods. The southeastern Bering Sea has high marine productivity along the shelf break, especially near marine canyons. At a hot spot located near Bering Canyon, we observed three foraging events over a 12 day period in June 2005. These were located by aerial surveys, quantified by airborne lidar and visual counts, and characterized by ship-based acoustics and net catches. Because of the high density of seabirds, the events could be seen in images from space-based synthetic aperture radar. The events developed at the shelf slope, adjacent to passes between the Aleutian Islands, persisted for 1 to 8 days, then abruptly disappeared. Build-up and break down of the events occurred on 24 hr time scales, and diameters ranged from 10 to 20 km. These events comprised large concentrations of euphausiids, copepods, herring, other small pelagic fishes, humpback whales, Dall's porpoise, short-tailed shearwaters, northern fulmars, and other pelagic seabirds. The lidar

and acoustic remote sensing data demonstrated that prey densities inside the events were several times higher than those outside, indicating the importance of including events in forage fish surveys. This implies a need for either very intensive traditional surveys covering large expanses or for adaptive surveys guided by remote sensing. To our knowledge, this is the first time that an Alaskan hot spot was monitored with the combination of airborne and satellite remote sensing.

Keywords: ecological hot spots; aerial surveys; lidar; remote sensing; fisheries acoustics; marine food chains; seabirds; marine mammals; forage fish; Bering Sea; SAR

1. Introduction

Marine ecosystems are generally patchy, with regions of low and high diversity and/or productivity, with the latter containing “sites of critical ecosystem linkages between trophic levels” [1] known as ecological “hot spots”. Foraging at these hot spots is often ephemeral and hot spots can occur at fixed locations, e.g., a shelf break or coral reef, or at temporary ocean features, e.g., an eddy or seasonal front [2-6]. The ecological importance of these hot spot features is evident from the occurrence of high numbers of predators, including some endangered species, high biodiversity, and high trophic exchange of energy, which can be orders of magnitude higher than in locations outside the hot spot in time or space [7]. In some locations, the persistence or predictability of prey availability is important in maintaining hot spots [6,8,9] and in others, hot spots are linked to primary productivity that probably leads to high prey density [10]. New methods have been developed and more will likely be required to find, track and monitor these key features in the ocean [2,4].

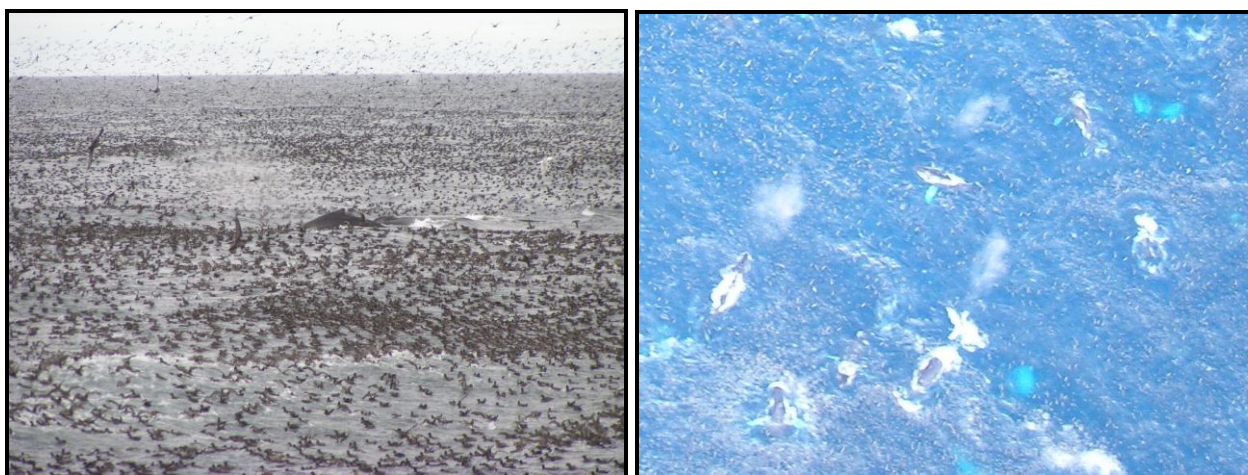
The sub-arctic Bering Sea is recognized as a region of extremes in seasonal productivity with regularly occurring hot spots [11-15]. Highly productive regions along the shelf break in the southern Bering Sea have been labeled the “green belt” [12]. Seven major canyons along this shelf break exhibit a strong influence on along-shelf and on-shelf transport [16-19]. The combination of strong tidal currents and steep bottom topography along the shelf edge, especially near the canyons, produces intense hot spots [5,6,20-22]. Of ten “meso-marine ecosystems”, mapped from British Columbia to Japan across the Gulf of Alaska and the Bering Sea over a multi-season and multi-year period, the region near Bering Canyon and Unimak Pass had the second highest chlorophyll concentrations, the highest mesoplankton densities, and the second highest seabird density [23].

Documentation of hot spot activity and processes in the Bering Sea greenbelt is limited because of difficulties in accessing remote locations and because of extremes in weather. Field study logistics and data collection are often limited by weather. New techniques with improved spatial and temporal coverage that can maximize data collection during optimal weather days or that can operate from a distant location will likely improve our ability to observe and document hot spots in remote, harsh environments such as the Bering Sea or over vast stretches of the open ocean.

In 2005, we studied a key hot spot near Bering Canyon using (1) space-borne SAR (Synthetic Aperture Radar), (2) airborne visual observations and lidar and (3) ship-based acoustics, visual species

identifications, and net sampling. Here we describe the evolution and size of foraging events (Figure 1) that were detected by airborne remote sensing within this hot spot and we investigate environmental factors affecting their evolution.

Figure 1. Photographs of foraging taken from the surface vessel and from the aircraft. In the left frame, the small dark objects on the surface are shearwaters, and there is a humpback whale diving in the center of the frame. See also the cover illustration on Issues 2–4, Volume 68, 2006 of *Progress in Oceanography*. In the right frame, the small light objects are seabirds, and seven humpback whales are visible.



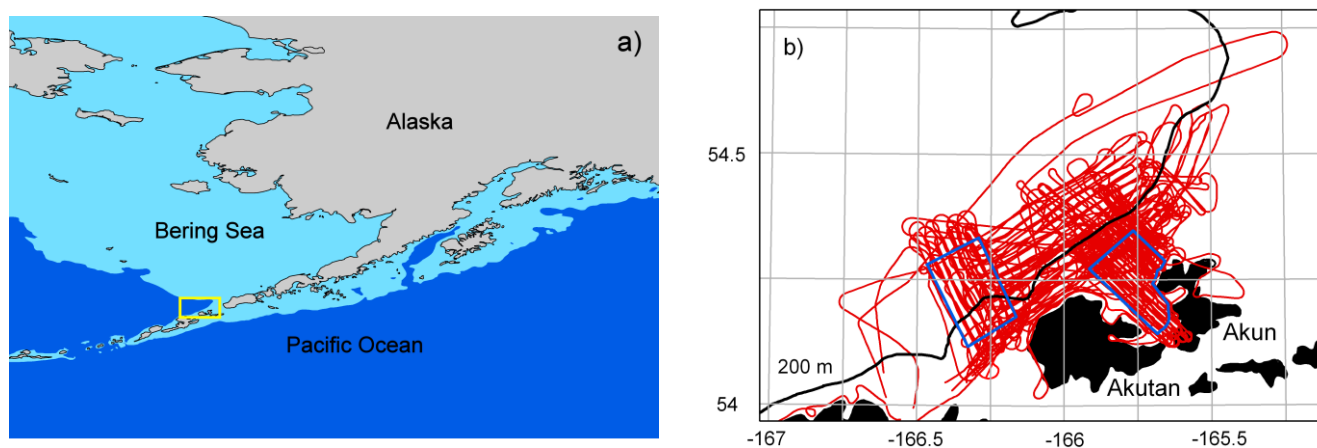
2. Methods

This study was conducted in the southeastern Bering Sea along the northern coasts of Akutan and Akun Islands (Figure 2). Repeat lidar and visual surveys were flown at an altitude of 305 m on a twin-engine aircraft at airspeeds between 120 and 160 knots between 8 and 19 June, 2005. Surveys were flown within a 120 by 60 km rectangle including continental shelf and slope habitats. Aerial transects were flown onshore to offshore and back within ship survey areas and within foraging event regions at a spacing ranging from 550 to 750 m. Wide-area search transects were also conducted parallel to the shelf and shorelines bisecting the ship tracks at a wider spacing of 4 to 5 km. In total, we flew about 7,900 km over the 12 day sampling period with two weather days resulting in eight daytime and three nighttime aerial surveys.

The lidar system on the aircraft, described in detail by Churnside *et al.* [24], was a non-scanning, radiometric lidar with three major components: (1) the laser and beam-control optics, (2) the receiver telescope, associated optics, and detector, and (3) the data collection and display computer. The laser was linearly polarized and the beam diverged, using a lens in front of the laser, to meet eye-safety standards established for marine mammals [25]. The resulting spot diameter on the surface, and hence the sampling swath width, was 5 m. A polarizer in front of the telescope selected the cross-polarized component of the reflected light to maximize the contrast between larger particles, like fish and large plankton, and smaller light-scattering particles, like small plankton and suspended sediments [26,27]. An interference filter at the rear of the telescope was used to reduce the amount of background light reaching the detector. An aperture at the focus of the primary lens also limited background light by

limiting the field of view of the telescope to match the divergence of the transmitted laser beam. The resulting light was incident on a photomultiplier tube, which converted the light into electrical current. The photomultiplier tube output was passed through a logarithmic amplifier to increase the dynamic range of the signal. A 50- Ω load resistor converted the current to voltage, which was digitized in the computer and stored, along with the time and position.

Figure 2. Study area in SE Bering Sea. **(a)** Chart of southwestern Alaska, showing the Bering Sea and Pacific Ocean, separated by the Alaska Peninsula and Aleutian Islands. The light and dark blue regions show where the water depth is <200 m and >200 m, respectively, and the location of the detailed chart is shown by the yellow rectangle. **(b)** A detailed chart of the region around Akutan and Akun Islands, with the 200 m bottom contour (black line), all flight tracks (red lines), and the ship's preselected systematic acoustic survey areas (blue lines), with the slope area on the left and shelf on the right.



Lidar data were inspected visually to identify fish schools [28-31] and plankton layers [32-34] using the characteristics of the returned signals observed in these studies. Background scattering levels and attenuation were estimated using the lidar returns in the vicinity of the schools, and a corrected backscattering strength was calculated. Corrected backscattering strength, position, time of observation, length, depth, and thickness of each school were recorded. The penetration depth of the lidar was also estimated by noting the depth at which the background scattering level was at the system noise level. A relative measure of each school size (relative index of abundance) was obtained by integrating the corrected backscattering strength over depth and along-track distance. In this way, the variation of fish density among schools was included. Since the lidar spot size was fixed at 5 m, the total lidar survey area for each transect was 5 m times the transect length.

Survey flights were also used to quantify the distribution of seabirds and marine mammals. Visual counts of seabirds and mammals followed protocols established during similar surveys [32], with time of observation related to GPS location data. To obtain a population estimate from these counts would require the effective visual detection strip width, which varies with target species and with ambient conditions [35]. A typical transect width for objects in the water is about 500 m from the aircraft at an altitude of 300 m [36], which corresponds to a view angle of 60° from nadir. No estimate of detection width was made here, and no estimates of total populations will be made.

From the aerial survey data, several density estimates were calculated. First, lidar was used to estimate the density of fish school number (schools km^{-1}) for the slope and shelf areas by the number of schools within each area divided by the total length of the flight track within each area. To account for differences in school size and density, we estimated the relative abundance of fish as the integral of the scattering strength over the school along the flight track. Second, using lidar and visual counts of foraging animals, we mapped the density of fish relative abundance (km^{-1}), mammals (number km^{-1}), and birds (number km^{-1}) over the entire survey region with a spatial resolution of 2 km by 2 km. These quantities, the number of birds, and the number of mammals for each spatial bin, were divided by the length of the flight track within that bin to get a relative density. Finally, we identified three rectangular boxes within the region of highest densities for a day by day analysis of fish, seabird and marine mammal densities. These densities were estimated for a box in the center of the hot spot (CEN), one just to the northeast (NE), and one just to the southwest (SW). A fourth box (NW), adjacent to the others, but outside of the region of highest concentrations, was also included in the analysis.

Systematic acoustic surveys were conducted in continental shelf (ocean depth < 100 m) and slope (depth 100–1,200 m) areas aboard the 38 m stern trawler, F/V *Great Pacific* (Figure 2). The slope area was surveyed 10–13 June 2005 and shelf area during 14–19 June 2005. Shelf transects were spaced 926 m (0.5 nmi) apart and slope transects were spaced 1.852 km (1.0 nmi) apart. Fish and macro-invertebrates were intermittently sampled using nets at locations where the reflected acoustic energy (*i.e.*, backscatter) was high. A total of 375 km of acoustic data were collected within the two systematic survey areas. In addition, the ship surveyed another 130 km within the hot spot region identified from the aircraft on 13, 14, 16, and 17 June.

Acoustic data were collected using a 38-kHz splitbeam echosounder (Simrad EK60 echosounder with ES38-12 transducer, pulse duration 1.024 ms, ping rate 1 s^{-1}). We installed the transducer on a towed body (YSI, Inc.) suspended 2.5 m below the water surface and towed it at approximately 3.1 m s^{-1} . Accounting for transducer depth and saturation, acoustic data were usable from depths greater than 6 m below the water surface to 0.5 m above the bottom. The echosounder was calibrated before our survey with a 38.1 mm tungsten carbide sphere using procedures outlined in [37].

Echoview (v 4.90, Myriax Pty Ltd, 2010) was used to analyze the acoustic data to obtain volume backscatter (S_v , dB re: 1 m^{-1}) and Area Backscatter Coefficient (ABC, $\text{m}^2 \text{ m}^{-2}$) as an index of combined plankton and fish density. Files were inspected for bottom detection, vessel noise spikes, and electrical interference prior to processing. Data from a SeaBird SBE-19 Seacat Conductivity-Temperature-Depth (CTD) casts during the survey were used to estimate absorption coefficients [38] and sound speed [39]. Vessel noise (-115 dB , S_v at 1 m) was removed from all data sets using linear subtraction [40,41]. A minimum S_v threshold of -82 dB was selected based on the calculated noise level at our maximum analytic depth of depth of 75 m. Samples with S_v values less than either our estimated vessel noise or our S_v minimum threshold were assigned -999 dB (effectively equivalent to zero backscatter in the linear domain; Myriax Pty Ltd, 2010). Acoustic data were divided into 100 m horizontal bins and two vertical bins: 6–30 m and 30–75 m. An average acoustic backscatter (ABC) value was calculated for the systematic shelf and slope surveys, the hot spot survey, and for all data (systematic + hot spot) based on the 6–30 and 30–75 m vertical bins.

Target aggregations observed in acoustic echograms were sampled using a Cantrawl 400/580 midwater trawl (5.0 m² alloy doors, 12 mm mesh codend liner, 15–18 m height, 55–60 m width). Trawl depth was monitored real-time using a netsonde on the headrope. Trawl duration lasted between 10 and 81 minutes, depending on target density observed with the acoustics. Upon net retrieval, the catch was identified to species, counted, and weighed. When catch volume was high, we subsampled by selecting a random portion of the trawl catch to count and weigh by species. The remainder of the catch was weighed, and the species composition of the whole catch extrapolated from the subsample. Weights were adjusted to obtain equivalent values for a standard 30-minute trawl duration.

Zooplankton and ichthyoplankton were sampled with a 0.25 m² multiple opening/closing MultiNet®, MN (HydroBios) equipped with five 335 µm mesh net bags. Two flow meters, one located inside the net opening and one located outside, were used to monitor the volume of water filtered. The MN was fished in a double oblique manner; plankton was collected over five depth ranges on the up-cast. Upon retrieval, the five nets were rinsed, cod-ends were detached and samples concentrated in sieves of the appropriate mesh size. Subsamples of major zooplankton taxa were collected and immediately frozen at –20 °C for further analyses of energy density. The remainders of the concentrated samples were fixed in 5% formalin seawater solution and returned to the University of Alaska Fairbanks laboratory in Juneau for further processing.

At the Juneau laboratory, zooplankton samples were scanned for large organisms, such as jelly fish and cephalopods, which were removed, identified to the lowest feasible taxonomic level and counted. The remaining samples were split with a Folsom plankton splitter until a sample size of approximately 100 specimens of the most abundant taxonomic group was achieved. In this split, all individuals of the abundant taxonomic groups were identified to the lowest level and developmental stage feasible and counted. The larger sub-samples were scanned for the less abundant taxa, which were identified and counted. Zooplankton energy content was analyzed using a Parr 1425 semi-micro bomb calorimeter. Prior to sample analysis, energy equivalent (EE) values were generated from 10 benzoic acid pellets with certified energy content on each of the 2 bomb units.

To determine if foraging events could be detected by satellite remote sensing, standard-mode (swath width = 100 km; resolution = 30 m) SAR data from the RADARSAT-1 satellite were obtained from the Alaska SAR Facility at the University of Alaska, and processed using software available from the same source. SAR images of the ocean surface show variations in radar reflectivity primarily caused by changes in sea surface roughness [42–44]. These include ship wakes [45] and schools of tuna [46].

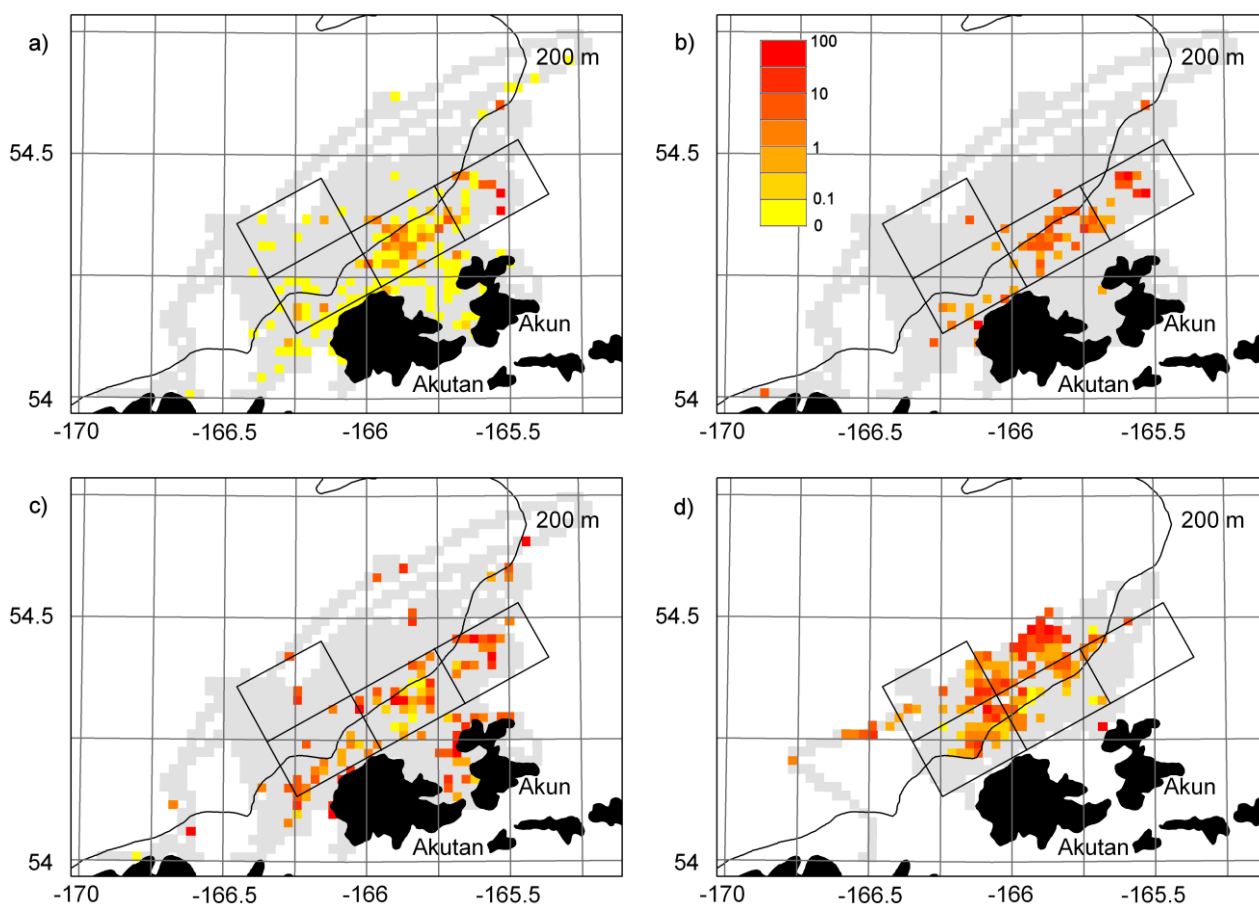
To compare the biological observations to physical factors, wind and tide data were regressed against aerial observation data. Hourly wind speed data (<http://www.wunderground.com/>) and six minute local tide height data (<http://tidesandcurrents.noaa.gov/>) measured at Unalaska, Alaska were used to develop wind variables and tide variables. Mean winds were estimated during the survey periods and for a six hour period immediately preceding survey periods. Wind mixing was estimated by calculating the cube of each wind speed measurement, a proxy used to represent energy needed for vertical mixing [47]; mean wind mixing was also estimated for the six hour period immediately before each survey periods. The final wind variables estimated were the mean north and east components during each survey period. Tide height was the tide level for the mid-point time of the flight. The time derivative of the six minute tide height data was used as a proxy for tidal flux. Seabird, marine

mammal and fish school observations were related to each other and to wind and tide variables using the Pearson correlation coefficients (r) and significance levels (p) were estimated using a two-sided Student's t test. Only correlations with $p < 0.05$ are reported as significant. The Bonferroni correction for multiple hypothesis tests reduces the threshold significance level by the number of hypotheses [48]. Results are reported with and without this correction.

3. Results

The aerially-mapped spatial distributions of fish, seabirds, and marine mammals indicate large concentrations during the day just outside of the bay between Akutan and Akun Islands (Figure 3). At night, the distribution of fish changed, with high numbers of fish and plankton rising to the surface waters beyond the shelf break; peak fish densities occurred during night surveys.

Figure 3. Spatial distributions of (a) birds, (b) marine mammals, (c) daytime fish, and (d) nighttime fish from aerial surveys. In each case, the relative density in each 2 km by 2 km bin was plotted as a percent of the highest value according to the logarithmic color scale in (b). Bins with no detections are in gray. The four rectangular boxes are those used for the hot-spot analysis, and the black line denotes the 200 m depth contour.



The highest concentrations of fish near the surface were observed outside the preselected intensive-survey areas (Table 1, Figure 3). The table shows that the average density of schools detected by the lidar over the total region was four times as large as that in either the slope or shelf areas. The

highest concentration during the day occurred at the shelf break, but to the northeast of the slope area. The highest concentration at night was located 14 km from the shelf break and was 8.6 times the highest daytime density. The total average acoustic energy was much closer to the values in the slope and shelf areas than were the lidar results, most likely because most of the acoustic survey effort was in those areas. The lidar and 6–30 m acoustic data both show shelf values that were slightly greater than the slope values, but the differences are within the uncertainties in the measurements. Acoustic signals within the hot spot were about five times the average of the total survey.

Table 1. Average number of schools per km detected by the lidar and Area Backscatter Coefficient (ABC, $\text{m}^2 \text{m}^{-2}$) measured by the echosounder in two depth bins for the total region surveyed, the slope area, and the shelf area as in Figure 2. Also presented are acoustic data collected in the hot spot on June 13 (year day 165.0).

| | Lidar (schools km^{-1}) | Acoustics (ABC 6–30 m) | Acoustics (ABC 30–75 m) |
|----------|-----------------------------------|----------------------------------|----------------------------------|
| Total | 0.105 ± 0.004 | $(1.13 \pm 0.17) \times 10^{-5}$ | $(9.63 \pm 1.42) \times 10^{-6}$ |
| Slope | 0.023 ± 0.005 | $(9.86 \pm 0.55) \times 10^{-6}$ | $(7.02 \pm 0.23) \times 10^{-6}$ |
| Shelf | 0.024 ± 0.004 | $(1.23 \pm 0.29) \times 10^{-5}$ | $(1.16 \pm 0.25) \times 10^{-5}$ |
| Hot spot | — | $(5.80 \pm 2.36) \times 10^{-5}$ | $(4.67 \pm 2.26) \times 10^{-5}$ |

The spatial and temporal evolution of foraging events, defined by high densities of seabirds, marine mammals, and associated fish schools, was recorded (Supplemental Material, Table S1) for the boxes denoted in Figure 3. An example of lidar data from 13 June 2005 (Figure 4) shows high densities of seabirds at and above the surface. Also in Figure 4 is a school of fish that extends from a depth of about 25 m to the limit of the lidar detection range at 50 m. Based on the acoustic data (Figure 5) and on associated net sampling, it is likely that these were either walleye pollock (*Theragra chalcogramma*) or Pacific herring (*Clupea pallasii*), which have frequently been observed feeding on euphausiids in the region (GLH, personal observations). Not visible on this scale in Figure 4 is a zooplankton layer that generally extended from the surface down to a depth of about 2 m. Because we could not reliably discriminate between this layer and seabirds at the surface from the lidar data, we were not able to investigate the spatial and temporal distribution of this zooplankton layer.

During daylight, the central box, just north of Akutan Bay, had the highest consistent densities of fishes, seabirds, and marine mammals. Although there was only limited overlap between ship surveys and aerial surveys within the hot-spot region shown in Figure 3, average acoustic backscatter values representing fish and plankton biomass were highest in the same region (the central box, between Akutan and Akun Islands, in Figure 3) that also had the consistently highest values for fish determined from lidar. Temporal comparisons of acoustics and lidar were unfortunately not possible because of the limited number of overlapping ship surveys.

Figure 4. Gray-scale plot of lidar return as a function of depth and distance along the flight track for a 2,000 m segment of data during the large foraging event on 13 June.

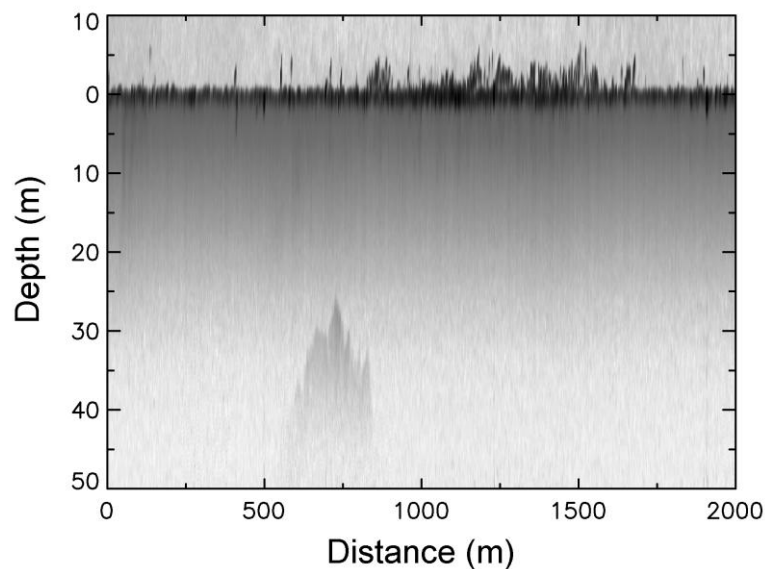
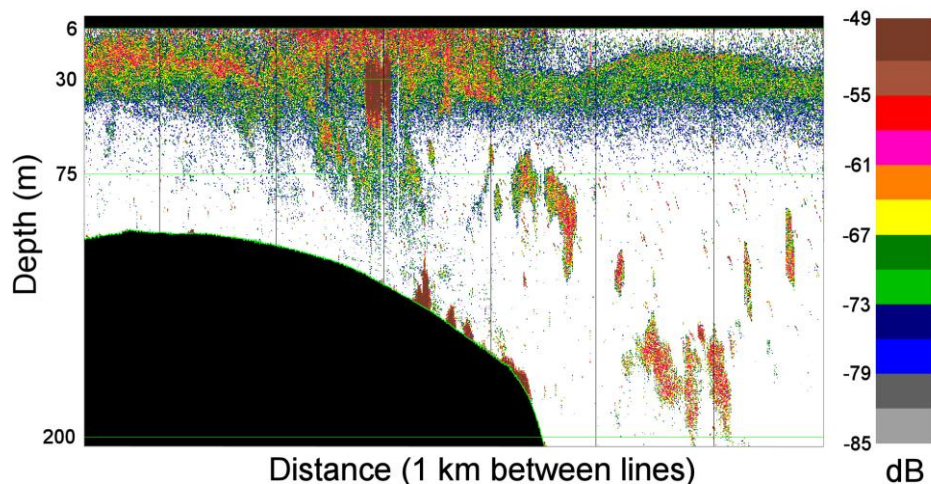


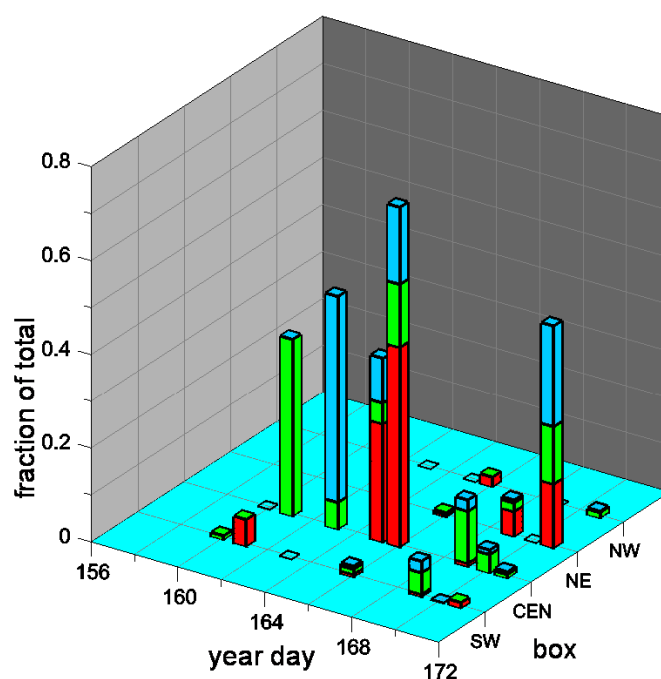
Figure 5. Acoustic echogram (daytime) of hot spot in the central box of Figure 3, with the surface (surface to 6 m depth) and bottom (0.5 m from the bottom and below) shown in black. Biological backscatter, from fish and plankton, are scaled from grey (low biomass) to brown (high biomass). Based on aggregation structure and the acoustic frequency used (38 kHz), the layer located between 6 and 50 m is likely dominated by plankton and the discrete aggregations within and below the layer are likely fish or euphausiids.



The temporal evolution of the foraging events (Figure 6) began with the observation of a high number of marine mammals in the central box on the afternoon of 9 June (local time; decimal year day 160.9 UTC). Two days later, on 11 June (year day 163.0), there were fewer marine mammals in the central box, but thousands of seabirds. The extent of the seabirds, used as a proxy value for the spatial extent of the event, was initially 10 km. On 13 June (year day 165.1), high numbers of fish schools, seabirds, and marine mammals were all present with even more activity on the next day (14 June, year day 165.9). On that same day, a second foraging event appeared to the southwest containing high

numbers of fish schools and associated marine mammals. By 17 June (year day 169.0), both foraging events were diminished and by the next day, the second one had disappeared. During the last survey day, 19 June (year day 170.8), a third event emerged along with the one originally observed. In these events, 97% of the birds were identified as dark shearwaters, most of which were probably short-tailed shearwaters (*Puffinus tenuirostris*). Of the marine mammals identified, 79% were humpback whales (*Megaptera novaeangliae*). A list of numbers by species is included in Table S3 in the Supplemental Material. Pacific herring were the eighth most common species caught by midwater trawl in the overall study, but were not captured in any of the hot spot trawls shown in Table S2. Within the depth sampled by lidar (<50 m), the most common species caught in the hot spot trawls were walleye pollock (51% by weight), pink salmon (*Onchorhynchus gorbuscha*) (14%) and jellyfish (*Scyphozoa*) (6%). One forage event was sampled using the aircraft to direct the tow (haul 7); walleye Pollock (39%) and chum salmon (*Onchorhynchus keta*) (60%) were the most common species caught. One school, most likely Pacific herring, was observed with the acoustic system mounted on the net diving below the net and thus avoiding capture.

Figure 6. Fraction of the total estimated number of seabirds (blue), marine mammals (green), and fish (red) observed in the Southwest (SW), Central (CEN), Northeast (NE), and Northwest (NW) boxes of Figure 3 during each daytime flight plotted as a function of the time of the flight in decimal year day (UTC).



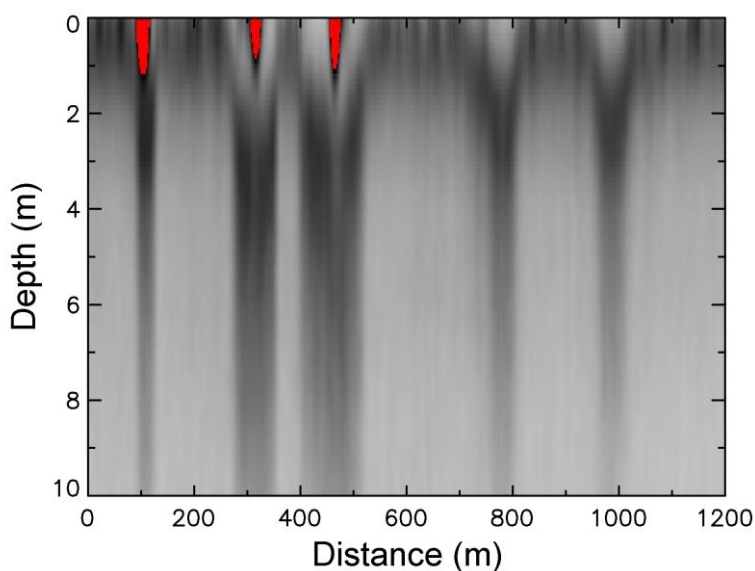
As Figure 6 suggests, there was a high degree of spatial correlation between daytime observations of fish and birds ($r = 0.997$; $p = 0.003$), fish and mammals ($r = 0.996$; $p = 0.004$), and birds and mammals ($r = 0.989$; $p = 0.011$) averaged over the four boxes. These correlations are still significant if we apply the Bonferroni correction, which requires that $p < 0.017$. If we add the temporal element by breaking out the data by box and flight, the resulting correlations are not significant at the 5% level. This is also evident in Figure 6, which shows that the greatest numbers of birds, marine mammals, and fish were observed on different days. Combining the data from all four boxes and looking at only temporal

correlations, we found that the only significant correlation ($r = 0.72$; $p = 0.046$) was between fish and birds densities. This result is not significant when the correction is applied.

The only significant correlation (at the 5% level) between the aerial observations and the environmental parameters was between the fish density and the easterly component of the mean wind ($r = 0.74$; $p = 0.037$). This correlation was largely the result of a shift in the wind from westerly to easterly on June 13, just before the large concentrations of fish were observed on 14 and 15 June. Because of the large number of environmental variables, this investigation involved ten hypotheses. With the Bonferroni correction, $p < 0.005$ would be required, and this result would not pass the more stringent test.

Generally, it was difficult to identify the source of lidar returns from very close to the surface, since specular reflections from the surface and scattering from bubbles near the surface cannot be excluded, even with a polarization filter that transmits less than 0.1% of the copolarized light from these sources. However, we frequently observed a two meter thick layer at the surface that would move deeper into the water column when there were birds on the surface (Figure 7). Our hypothesis is that these were large zooplankton diving to avoid predation by birds at the surface. This hypothesis is supported by visual observations of birds regurgitating euphausiids as the ship approached. Also, the presence of these layers on a given flight was significantly correlated with average winds of less than 3 m s^{-1} ($r = 0.37$, $p = 0.018$). In light winds, there are few wave slopes at the 15° incidence angle of the lidar and few breaking waves to produce near-surface bubbles. The turbulence near the surface would also be lower, which would allow plankton layers to form and to persist.

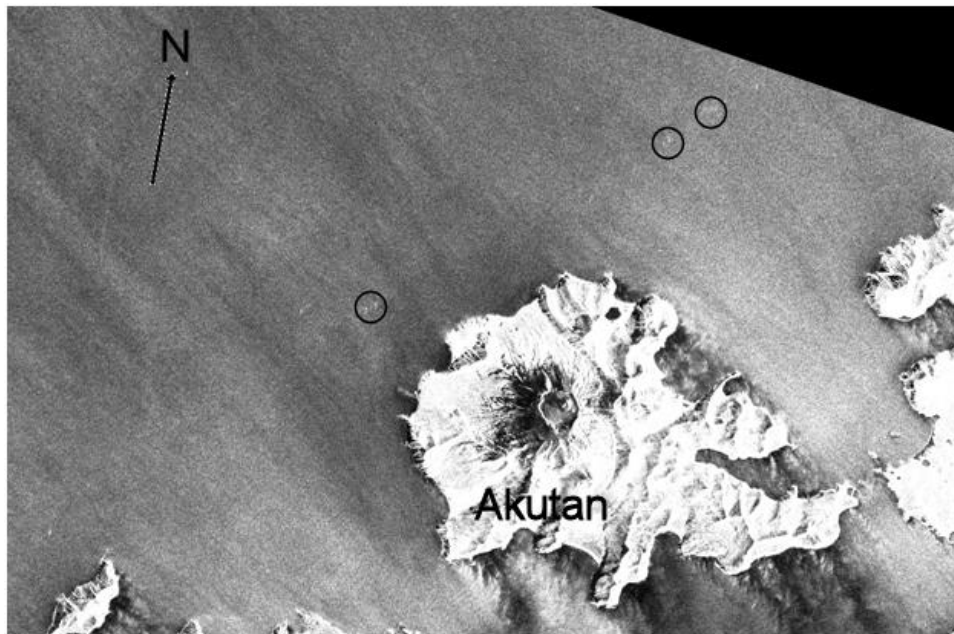
Figure 7. Gray-scale plot of lidar return as a function of depth and distance along the flight track for a 1,200 m segment of data during the large foraging event on 9 June. Contrast has been increased to increase visibility, resulting in saturation of the return from birds at the surface (red).



The size of the foraging event on 11 June was large enough to be observed from space and foraging events occurred on the edge of a front detected by satellites. On 11 June, peak seabird density occurred in the central box (Figure 3) and affected surface roughness on a scale consistent with that observed in

a SAR image (Figure 8). The bright regions in the SAR return are between 100 m and 1 km in extent, consistent with the length of the region of greatest activity in Figures 3 and 6. At this point, it is not clear if flocks of seabirds produce a characteristic SAR signature that can be reliably identified in the presence of other sources of enhanced scattering.

Figure 8. SAR image of Akutan Island and the hot spot region to the north taken on June 11. Image is 61 km left to right and 41 km top to bottom. Circles showing most intense backscatter are 2 km in diameter. (© CSA 2005).



4. Discussion and Conclusions

To our knowledge, this is the first time the evolution and temporal variability of a large foraging event at a known Bering Sea hot spot has been documented using airborne remote sensing and surface-vessel measurements. Observations and measurements of the biological activity consisting of zooplankton, fish, seabirds, and marine mammals were accomplished using aerial surveys including lidar; these measurements revealed distributions patterns of birds and prey and their interactions in three dimensions. It is also the first time that a documented foraging event was recognized in satellite imagery, although physical locations of hot spots have frequently been documented using space-borne sensors [4,49].

The species composition of seabirds and marine mammals that we observed is similar to what has been reported by others. The domination of foraging events by short-tailed shearwaters at the eastern end of the Aleutian Chain has been reported in the past [20,22,50], as has the common occurrence of northern fulmar there [20,23]. Humpback whales have also been recorded in the region [15,51], and there is much anecdotal information associating whales with seabirds.

While the largest numbers of zooplankton were copepods, the larger euphausiids had greater total energy content. On the shelf, 430 copepods m^{-3} were counted, but only 55 euphausiids m^{-3} . However, these euphausiids contained 12 $kJ m^{-3}$ and the copepods only 7 $kJ m^{-3}$. In the southeastern Bering Sea and eastern Aleutian Islands, euphausiids are a major food source for shearwaters [13,22,50,52] and

humpback whales [53]. The relative contribution of copepods and euphausiids to the lidar return is not known, and more work on relative scattering cross sections of these two groups is needed. The combination of steep slope, large tidal fluxes, mixing of nutrient-laden Pacific and Bering Sea waters, and considerable water mass exchange in Aleutian passes is known to create a biological hot spot in the region of our observations [20-23,54].

At the beginning of our observations, on 9 June, winds were light, and there was a wide-spread surface layer of euphausiids. Fish, whales, and birds were associated with this surface layer of euphausiids, although the highest concentrations of fish, whales and seabirds were at different locations, and only whales were present at high densities. On 12 June, the wind increased and shifted to the east. Over the next few days, there was a large increase in activity, with fish, whales, and birds all observed in the same regions. We hypothesize that the easterly winds would have the effect of creating an offshore flow at the surface due to Ekman transport, and an on-shelf flow of water at depth. These flows could have brought higher numbers of euphausiids onto the shelf where we observed the greatest biological activity. Renner *et al.* [55] have suggested a North Pacific source for the euphausiids. Along the north side of the Aleutian Islands is the Aleutian North Slope Current that transports water, originating in the Gulf of Alaska, from the major passes to the west. Near the study region, it turns sharply to the northwest to become the Bering Slope Current that runs along the edge of the eastern Bering Sea shelf. Renner *et al.* hypothesize that the euphausiids originate along the slope and shelf of the western Gulf of Alaska, and that they are carried first westward and then northward through the deep passes in the central Aleutian Islands (especially Amukta Pass), and thence into the Aleutian North Slope Current.

The foraging event documented in this study appeared to start within the central box of the hot spot (Figure 6) which exhibited the most consistently high numbers of fish schools, seabirds, and marine mammals, as well as high densities of zooplankton. Based on these observations, we suggest that the central box represents the core region for initialization of foraging events within the hot spot, probably due to peak prey densities, and these events spread and drifted to the northeast over the course of a few days until the event was over. Spreading and shifting could occur because of prey movement, depletion from grazing within the core region, or advection in the Aleutian North Slope Current [56]. This suggests that the ephemeral foraging events could be driven, in part, by pulses of prey brought into the region by a combination of transport in the Bering Slope Current and upwelling and on-shelf transport resulting from episodes of east winds.

Acknowledgements

Funding for this work was provided by the North Pacific Research Board (Project 401, NPRB paper 288) and the National Science Foundation (Grant OPP-0908262). We would like to thank Commander Northwest and our attentive pilot Marco Collela for providing a mechanically reliable aircraft and for protecting our safety, the Captain Charles “Jack” Bronson and crew of the vessel F/V *Great Pacific* for their generous support during the ship-based survey operations, and James Wilson for assistance with equipment engineering, installation, and operation.

References

1. Sydeman, W.J.; Brodeur, R.D.; Grimes, C.B.; Bychkov, A.S.; McKinnell, S. Marine habitat hotspots and their use by migratory species and top predators in the North Pacific Ocean: Introduction. *Deep-Sea Res. II* **2006**, *53*, 247-249.
2. Malakoff, D. New tools reveal treasures at ocean hot spots. *Science* **2004**, *304*, 1104-1105.
3. Worm, B.; Sandow, M.; Oschiles, A.; Lotze, H.K.; Myers, R.A. Global patterns of predator diversity in the open oceans. *Science* **2005**, *309*, 1365-1369.
4. Palacios, D.M.; Bograd, S.J.; Foley, D.G.; Schwing, F.B. Oceanographic characteristics of biological hot spots in the North Pacific: a remote sensing perspective. *Deep-Sea Res. II* **2006**, *53*, 250-269.
5. Coyle, K.O.; Hunt, G.L.; Decker, M.B.; Weingartner, T.J. Murre foraging, epibenthic sound scattering and tidal advection over a shoal near St. George Island, Bering Sea. *Mar. Ecol. Prog. Ser.* **1992**, *83*, 1-14.
6. Hunt, G.L., Jr.; Russell, R.W.; Coyle, K.O.; Weingartner, T.J. Comparative foraging ecology of planktivorous auklets in relation to ocean physics and prey availability. *Mar. Ecol. Prog. Ser.* **1998**, *167*, 241-259.
7. Yen, P.P.W.; Sydeman, W.J.; Bograd, S.J.; Hyrenbach, K.D. Spring-time distributions of migratory marine birds in the southern California Current: Oceanic eddy associations and coastal habitat hotspots over 17 years. *Deep-Sea Res. II* **2006**, *53*, 399-418.
8. Gende, S.M.; Sigler, M.F. Persistence of forage fish 'hot spots' and its association with foraging Steller sea lions (*Eumetopias jubatus*) in southeast Alaska. *Deep-Sea Res. II* **2006**, *53*, 432-441.
9. Hunt, G.L., Jr.; Mehllum, F.; Russell, R.W.; Irons, D.; Decker, M.B.; Becker, P.H. Physical processes, prey abundance, and the foraging ecology of seabirds. In *Proceedings of the International Ornithological Congress 22*, Durban, South Africa, 16–11 August 1998; pp. 2040-2056.
10. Suryan, R.M.; Sato, F.; Balogh, G.R.; Hyrenback, K.D.; Sievert, P.R.; Ozaki, K. Foraging destinations and marine habitat use of short-tailed albatrosses: A multi-scale approach using first-passage time analysis. *Deep-Sea Res. II* **2006**, *53*, 370-386.
11. Naumenko, E.A. Distribution, biological condition and abundance of capelin (*Mallotus villosus socialis*) in the Bering Sea. In *Ecology of the Bering Sea: A review of Russian Literature*; Mathisen, O.A., Coyle, K.O., Eds.; Alaska Sea Grant College Program: Fairbanks, AK, USA, 1996; Rpt. 97/01, pp. 237-256.
12. Springer, A.M.; McRoy, C.P.; Flint, M. The Bering Sea green belt. *Fish. Oceanogr.* **1996**, *5*, 205-223.
13. Hunt, G.L., Jr.; Coyle, K.O.; Hoffman, S.; Decker, M.B.; Flint, E.N. Foraging ecology of the short-tailed shearwaters near the Pribilof Islands, Bering Sea. *Mar. Ecol. Prog. Ser.* **1996**, *141*, 1-11.
14. Hunt, G.L., Jr.; Kato, H.; McKinnell, S.M. *Predation by Marine Birds and Mammals in the Subarctic North Pacific Ocean*; Scientific Report 14; PICES: Sidney, BC, Canada, 2000; p. 165.
15. Sinclair, E.H.; Stabeno, P.J. Mesopelagic nekton and associated physics in the southeastern Bering Sea. *Deep-Sea Res. II* **2002**, *49*, 6127-6146.

16. Stabeno, P.J.; Schumacher, J.D.; Ohtani, K. The physical oceanography of the Bering Sea. In *Dynamics of the Bering Sea*; Loughlin, R.R., Ohtani, K., Eds.; Alaska Sea Grant College Program: Fairbanks, AK, USA, 1999; Rpt. AK-SG-99-03, pp. 1-28.
17. Stabeno, P.J.; Kachel, N.; Mordy, C.; Righi, D.; Salo, S. An examination of the physical variability around the Pribilof Islands in 2004. *Deep-Sea Res. II* **2008**, *55*, 1701-1716.
18. Mizobata, K.; Wang, J.; Saitoh, S.-I. Eddy-induced cross-slope exchange maintaining summer high productivity of the Bering Sea shelf break. *J. Geophys. Res.* **2006**, *111*, C10017, doi: 10.1029/2005jc003335.
19. Mizobata, K.; Saitoh, S.-I.; Wang, J. Interannual variability of summer biochemical enhancement in relation to mesoscale eddies at the shelf break in the vicinity of the Pribilof Islands, Bering Sea. *Deep-Sea Res. II* **2008**, *55*, 1717-1728.
20. Ladd, C.; Jahncke, J.; Hunt, G.L.; Coyle, K.O.; Stabeno, P.J. Hydrographic features and seabird foraging in the Aleutian Passes. *Fish. Oceanogr.* **2005**, *14* (Suppl. 1), 178-195.
21. Piatt, J.F.; Wetzel, J.; Bell, K.; DeGange, A.R.; Balogh, G.R.; Drew, G.S.; Geernaert, T.; Ladd, C.; Byrd, G.V. Predictable hotspots and foraging habitat of the endangered short-tailed albatross (*Phoebastria albatrus*) in the North Pacific: Implications for conservation. *Deep-Sea Res. II* **2006**, *53*, 387-398.
22. Jahncke, J.; Coyle, K.O.; G.L. Hunt, G.L., Jr. Seabird distribution, abundance and diets in the central and eastern Aleutian Islands. *Fish. Oceanogr.* **2005**, *14* (Suppl. 1), 160-177.
23. Batten, S.D.; Hyrenback, K.D.; Sydeman, W.J.; Morgan, K.H.; Henry, M.F.; Yen, P.Y.; Welch, D.W. Characterizing meso-marine ecosystems of the North Pacific. *Deep-Sea Res. II* **2006**, *53*, 270-290.
24. Churnside, J.H.; Wilson, J.J.; Tatarskii, V.V. An airborne lidar for fisheries applications. *Opt. Eng.* **2001**, *40*, 406-414.
25. Zorn, H.M.; Churnside, J.H.; Oliver, C.W. Laser safety thresholds for cetaceans and pinnipeds. *Mar. Mammal Sci.* **2000**, *16*, 186-200.
26. Churnside, J.H.; Wilson, J.J.; Tatarskii, V.V. Lidar profiles of fish schools. *Appl. Opt.* **1997**, *36*, 6011-6020.
27. Lewis, G.D.; Jordan, D.L.; Roberts, P.J. Backscattering target detection in a turbid medium by polarization discrimination. *Appl. Opt.* **1999**, *38*, 3937-3944.
28. Churnside, J.H.; Demer, D.A.; Mahmoudi, B. A comparison of lidar and echosounder measurements of fish schools in the Gulf of Mexico. *ICES J. Mar. Sci.* **2003**, *60*, 147-154.
29. Carrera, P.; Churnside, J.H.; Boyra, G.; Marques, V.; Scalabrin, C.; Uriarte, A. Comparison of airborne lidar with echosounders: A case study in the coastal Atlantic waters of southern Europe. *ICES J. Mar. Sci.* **2006**, *63*, 1736-1750.
30. Churnside, J.H.; Tenningen, E.; Wilson, J.J. Comparison of data-processing algorithms for the lidar detection of mackerel in the Norwegian Sea. *ICES J. Mar. Sci.* **2009**, *66*, 1023-1028.
31. Churnside, J.H.; Demer, D.; Griffith, D.A.; Emmett, R.L.; Brodeur, R. D. Comparisons of lidar, acoustic and trawl data on two scales in the northeast Pacific Ocean. *CalCOFI Rep.* **2009**, *50*, 118-122.

32. Brown, E.D.; Churnside, J.H.; Collins, R.L.; Veenstra, T.; Wilson, J.J.; Abnett, K. Remote sensing of capelin and other biological features in the North Pacific using lidar and video technology. *ICES J. Mar. Sci.* **2002**, *59*, 1120-1130.
33. Churnside, J.H.; Thorne, R.E. Comparison of airborne lidar measurements with 420 kHz echo-sounder measurements of zooplankton. *Appl. Opt.* **2005**, *44*, 5504-5511.
34. Churnside, J.H.; Donaghay, P.L. Thin scattering layers observed by airborne lidar. *ICES J. Mar. Sci.* **2009**, *66*, 778-789.
35. Hobbs, R.C.; Waite, J.M. Abundance of harbor porpoise (*Phocoena phocoena*) in three Alaskan regions, corrected for observer errors due to perception bias and species misidentification, and corrected for animals submerged from view. *Fish. Bull.* **2010**, *108*, 251-267.
36. Pichel, W.G.; Churnside, J.H.; Veenstra, T.S.; Foley, D.G.; Friedman, K.S.; Brainard, R.E.; Nicoll, J.B.; Zheng, Q.; Clemente-Colon, P. Marine debris collects within the north Pacific subtropical convergence zone. *Mar. Pollut. Bull.* **2007**, *54*, 1207-1211.
37. Foote, K.G.; Knudsen, H.P.; Vestnes, G.; MacLennan, D.N.; Simmonds, E.J. *Calibration of Acoustic Instruments for Fish Density Estimation: A Practical Guide*; Cooperative Research Report No. 144; International Council for the Exploration of the Sea: Copenhagen, Denmark, February 1987; pp. 1-69.
38. Francois, R.E.; Garrison, G.R. Sound absorption based on measurements. Part II: Boric acid contribution and equation for total absorption. *J. Acoust. Soc. Am.* **1982**, *72*, 1879-90.
39. Chen, C.T.; Millero, F.J. Speed of sound in seawater at high pressures. *J. Acoust. Soc. Am.* **1977**, *62*, 1129-1135.
40. Watkins, J.L.; Brierley, A.S. A post-processing technique to remove background noise from echo-integration data. *ICES J. Mar. Sci.* **1996**, *53*, 339-344.
41. Korneliussen, R.J. Measurement and removal of echo integration noise. *ICES J. Mar. Sci.* **2000**, *57*, 1204-1217.
42. Vesecky, J.F.; Stewart, R.H. The observation of ocean surface phenomena using imagery from the SEASAT synthetic aperture radar: An assessment. *J. Geophys. Res.* **1982**, *87*, 3397-3430.
43. Ivanov, A.; Ginzburg, A. Oceanic eddies in synthetic aperture radar images. *J. Earth Syst. Sci.* **2002**, *111*, 281-295.
44. Kerbaol, V.; Collard, F. SAR-Derived coastal and marine applications: from research to operational products. *IEEE J. Oceanic Eng.* **2005**, *30*, 472-486.
45. Reed, A.M.; Milgram, J.H. Ship wakes and their radar images. *Ann. Rev. Fluid Mech.* **2002**, *34*, 469-502.
46. Petit, M.; Stretta, J. M.; Farrugio, H.; Wadsworth, A. Synthetic aperture radar imaging of sea surface life and fishing activities. *IEEE Trans. Geosci. Remote Sens.* **1992**, *30*, 1085-1089.
47. Mann, K.H.; Lazier, J.R.N. *Dynamics of Marine Ecosystems; Biological-Physical Interactions of the Oceans*, 3rd ed.; Blackwell Science: Cambridge, MA, USA, 1991; p. 496.
48. Nakagawa, S. A farewell to Bonferroni: The problems of low statistical power and publication bias. *Behav. Ecol.* **2004**, *15*, 1044-1045.

49. Zainuddin, M.; Kiyofuji, H.; Saitoh, K.; Saitoh, S.-I. Using multi-sensor satellite remote sensing and catch data to detect ocean hot spots for albacore (*Thunnus alalunga*) in the northwestern North Pacific. *Deep-Sea Res. II* **2006**, *53*, 419-431.
50. Vlietstra, L.S.; Coyle, K.O.; Kachel, N.B.; Hunt, G.L., Jr. Tidal front affects the size of prey used by a top marine predator. *Fish. Oceanogr.* **2005**, *14* (Suppl. 1), 196-211.
51. Sinclair, E.H.; Moore, S.E.; Friday, N.A.; Zeppelin, T.K.; Waite, J.M. Do patterns of Steller sea lion (*Eumetopias jubatus*) diet, population trend and cetacean occurrence reflect oceanographic domains from the Alaska Peninsula to the central Aleutian Islands? *Fish. Oceanogr.* **2005**, *14* (Suppl. 1), 223-242.
52. Baduini, C.L.; Hunt, G.L., Jr.; Pinchuk, A.I.; Coyle, K.O. Patterns in diet reveal foraging site fidelity of short-tailed shearwaters in the southeastern Bering Sea. *Mar. Ecol. Prog. Ser.* **2006**, *320*, 279-292.
53. Pauly, D.; Trites, A.; Capuli, E.; Christensen, V. *Diet Composition and Trophic Levels of Marine Mammals*; Marine Mammal Committee/N:13; ICES C. M.: Aalborg, Denmark, 1995; p. 22.
54. Hunt, G.L., Jr.; Stabeno, P.J. Oceanography and ecology of the Aleutian Archipelago: Spatial and temporal variation. *Fish. Oceanogr.* **2005**, *14* (Suppl. 1), 292-306.
55. Renner, M.; Hunt, G.L., Jr.; Piatt, J.F.; Byrd, G.V. Seasonal and distributional patterns of seabirds along the Aleutian Archipelago. *Mar. Ecol. Prog. Ser.* **2008**, *357*, 301-311.
56. Stabeno, P.J.; Reed, R.K. Circulation in the Bering Sea basin observed by satellite-tracked drifters: 1986-1991. *J. Phys. Oceanogr.* **1994**, *24*, 848-854.

© 2011 by the authors; licensee MDPI, Basel, Switzerland. This article is an open access article distributed under the terms and conditions of the Creative Commons Attribution license (<http://creativecommons.org/licenses/by/3.0/>).